Journal of Alloys and Compounds 1018 (2025) 179203

Contents lists available at ScienceDirect

Journal of Alloys and Compounds

journal homepage: www.elsevier.com/locate/jalcom

Structural and magnetic states of $Fe_{100\text{-}x}Zr_x$ ($x = 6$–13 at%) films: Peculiarities verified by X-ray diffraction, Mössbauer and magneto-optical spectroscopies, and magnetometry

E.N. Sheftel[a], V.S. Rusakov[b], E.A. Gan'shina[b], E.V. Harin[a], V.A. Tedzhetov[a,*], D.M. Gridin[b], A.M. Gapochka[b], I.M. Pripechenkov[b], A.B. Granovsky[b,c]

[a] Baikov Institute of Metallurgy and Materials Science, Russian Academy of Sciences, Leninskii pr. 49, Moscow 119334, Russia
[b] Faculty of Physics, Lomonosov Moscow State University, Leninskie Gory 1, Moscow 119991, Russia
[c] Institute for Theoretical and Applied Electrodynamics Russian Academy of Science, ul. Izhorskaya 13, Moscow 125412, Russia

ARTICLE INFO

Keywords:
soft magnetic films
X-ray diffraction
Mössbauer spectroscopy
transverse Kerr effect
magneto-optical spectroscopy
magnetometry
hysteresis loop
PACS:
81.07.-b

ABSTRACT

The $Fe_{100\text{-}x}Zr_x$ (with $x = 6$–13 at%) films are formed on glass-ceramic substrates by ion-beam deposition. The structural and magnetic states of the films were analyzed using X-ray diffraction, Mössbauer and magneto-optical (based on transverse Kerr effect) spectroscopy, and magnetometry. All measurements were performed at room temperature for as-deposited films and the films annealed at 300 and 500°C. Analysis of the whole set of obtained data shows that a mixed (nanocrystalline + amorphous) structure forms in the films. The nanocrystalline phase is the Zr solid solution in α-Fe, α-Fe(Zr). The as-deposited films with the high Zr content ($x > 8.3$ at%) are characterized by dominant amorphous constituent, whereas the films with $x \leq 7.1$ at.% are nanocrystalline and characterized by a very low content of the amorphous constituent. Since, at room temperature, the α-Fe(Zr) phase is ferromagnetic and the amorphous one is paramagnetic, the magnetic properties of the films in the as-deposited and annealed states are determined by relative content of these structural constituents and by Zr content in the α-Fe(Zr) phase. This fact explains abrupt changes in the magnetic properties of the as-deposited films when x changes from 7.1 to 8.3 at% and an increase in the magnetization of the films with $x > 8.3$ at% after the annealing at 500°C leading to an increase in the nanocrystalline phase content.

1. Introduction

Nanocrystalline and amorphous ferromagnetic alloys are rather promising as soft magnetic materials for applications in modern magnetic microelectronics [1]. Iron-containing alloys are important in the design of such materials and form the basis for a new family of soft magnetic Fe-Me_{IV}-X films (where Me_{IV} are IVa Group metals and X is C, N, O, and B) with the nanocrystalline precipitation-strengthened structure [2]. In particular, Fe-Zr-N [3] and Fe-Ti-B-based [4,5] films with the nanocrystalline precipitation-strengthened structure formed in the course of magnetron deposition followed by the annealing can exhibit the high saturation magnetization, low coercive field, and high magnetic permeability at up to gigahertz frequencies and are characterized by the thermal stability of the structure, which make them competitive with amorphous and nanocrystalline soft magnetic materials prepared by the melt spinning [6–10].

As is known, materials prepared by melt spinning and sputtering are usually characterized by the so-called mixed structure that comprises the coexisting amorphous and nanocrystalline phases; in this case, the relationship between volume fractions of these phases affecting the main magnetic characteristics depends on the preparation method of material and technological parameters [6–8]. The control of the magnetic properties of such alloys requires a detailed understanding of their phase and structural states at the nanoscale [8–11].

A lot of publications on Fe-Zr alloys with Zr content of about 10 at% appeared 40 years ago in connection with the study of amorphous alloys, which are prepared by various methods, in particular, by melt spinning, sputtering, and mechanical alloying [9–12 and references therein]. In the studies of their magnetic properties using neutron diffraction, Mössbauer spectroscopy, and magnetometry [9–12], it was assumed that the alloys would be in an amorphous state. The revealed features of the magnetic properties were related to the inhomogeneous iron

---

* Corresponding author.
E-mail address: vtedzhetov@imet.ac.ru (V.A. Tedzhetov).

https://doi.org/10.1016/j.jallcom.2025.179203
Received 7 November 2024; Received in revised form 11 January 2025; Accepted 12 February 2025

distribution, which is intrinsic to the amorphous state. At room temperature, the studied amorphous $Fe_{100\text{-}x}Zr_x$ alloys were paramagnetic (the maximum Curie temperature does not exceed 226 K); as the temperature decreases, either uniform ferromagnetic state, or non-uniform ferromagnetic state with unidirectional anisotropy, or spin-glass state was formed depending on the Zr concentration [9–12]. The widespread interest in Fe-Zr alloys is related to the anomalous and abrupt change in their magnetic properties at certain Zr content. In addition, Fe-Zr alloys are spectacular representatives of a wide range of soft magnetic Fe-based alloys. In the course of our long-term studies of soft magnetic alloys based on Fe, in particular Fe-Zr-N, we realized that a complete understanding of the structural and magnetic properties of Fe-Zr alloys has not been achieved yet.

Taking into account the modern concept on the formation of mixed (amorphous + nanocrystalline) structure [6–8] in nanocrystalline alloys, it is of interest to study the structure of the $Fe_{100\text{-}x}Zr_x$ films with a wide Zr composition range using various mutually complementary methods.

In the present study, the structure at both macro and micro levels and magnetic properties of the $Fe_{100\text{-}x}Zr_x$ films with $x = 6.0–13.0$ at.% formed by the ion-beam deposition followed by annealing at 300 and 500°C are investigated using magneto-optical and Mössbauer spectroscopy, X-ray diffraction, and magnetometry. The analysis of the whole set of obtained experimental data allowed us to identify the complicated phase-structural and magnetic states of the films both in the bulk of the material and in its near-surface area.

2. Materials and methods

The $Fe_{100\text{-}x}Zr_x$ films with $x = 6.0$, 7.1, 8.3, 11, and 13 at% were obtained on glass-ceramic substrates (270 ×60 ×0.5 mm^3 in size, ST-50–0.6 grade) by ion-beam deposition using a Fe-Zr composite target. The target is a Zr sheet (280 ×80 mm^2 in size) coated with Fe stripes, the spacing between which increases from one end of target to the other, owing to the fact, the Fe-to-Zr ratio in the as-deposited films was varied. The films were deposited in an Ar atmosphere at $U = 20$ V and $I = 80$ mA. The film thickness values are listed in Table 1. A nanocrystalline Fe film was formed for comparison. Samples were annealed at 300 and 500°C for 1 h in a vacuum of no worse than $4{\cdot}10^{-4}$ Pa.

Table 1
Structural parameters obtained by XRD analysis of the $Fe_{100\text{-}x}Zr_x$ films.

x, at%	Thickness, µm	T_{an}, °C	Phase	Grain size D, nm	a, Å (using $2\theta_{max}$)
6.0	0.99	As-deposited	α-Fe(Zr) amorphous	20.0	2.898
		300	α-Fe(Zr) amorphous	25.1	2.896
		500	α-Fe(Zr) amorphous	19.9	2.878
7.1	1.27	As-deposited	α-Fe(Zr) amorphous	15.6	2.926
		300	α-Fe(Zr) amorphous	12.2	2.917
		500	α-Fe(Zr) amorphous	15.7	2.896
8.3	1.40	As-deposited	α-Fe(Zr) amorphous	7.2 2.4*	2.929
		300	α-Fe(Zr) amorphous	9.2 2.4*	2.923
		500	α-Fe(Zr)	10.7	2.871
11.0	1.52	As-deposited	amorphous	2.0*	
		300	amorphous	2.0*	
		500	α-Fe(Zr) amorphous	3.1 2.0*	2.875
13.0	1.43	As-deposited	amorphous	1.9*	
		300	amorphous	1.9*	
		500	α-Fe(Zr) amorphous	2.4 1.8*	2.879

* Fe-based amorphous phase in terms of XRD with ferromagnetic CDs/grains

The quantitative and qualitative phase analysis of the structure of the formed films was performed by X-ray diffraction technique. The studies were carried out using an Ultima IV (Rigaku, Japan) diffractometer equipped with a graphite monochromator, with the use of Bragg-Brentano geometry and CuK_α radiation. The diffraction patterns were taken in the 2θ angular range from 20° to 120° at a step of 0.2°.

To eliminate the contribution of substrate material to diffraction patterns, the diffraction pattern of glass-ceramic substrate was subtracted from all experimental diffraction patterns. The phase composition and volume fractions of crystalline phases and their lattice parameters a were determined by the Rietveld method [13]. The analysis of fine structure of the films (grain size D and the Gaussian root-mean square microstrain at the grain scale) was fulfilled by separation of block and strain broadening effects [14,15]; in this case, PHAN and PHAN% [16] software was used. Note that we determined the broadening associated with microstrain only to separate it from the broadening associated with grain size, and we do not discuss it further. Additionally, the lattice parameter a was calculated, and wide peaks were resolved into components, using positions of center of gravity ($2\theta_{max}$) of high-angle (211) and (220) reflections of α-Fe, via the fitting of patterns with the pseudo-Voigt function. The coherent domain, CD (short-range ordered area) or very fine grain size in the amorphous (in terms of X-ray diffraction) phase was determined by the Scherrer formula

$$D = \frac{\lambda}{\beta\cos\theta}, \tag{1}$$

where D is the coherent domain size and β is the integral angular width of the peak.

Static magnetic properties of the films were studied at magnetic fields up to 15 kOe using a LakeShore 7407 vibrating-sample magnetometer (VSM). The error of measuring of saturation magnetization did not exceed 10 %.

Magneto-optical (MO) properties of the films were studied in the transverse Kerr effect geometry. The transverse Kerr effect (TKE) is the relative intensity change of p-polarized light reflected from a sample upon its magnetization. Therefore, the field dependences of the TKE characterizes the magnetization process of near-surface layers, whereas the spectral dependences of TKE reveal specific features of the electron structure of films, which are related to their structural state [17]. This fact determines the possibilities of MO spectroscopy for the study of peculiarities of amorphous and nanocrystalline states, in particularly, of Fe-Zr films. Field dependences of the TKE were measured at different wavelengths at a magnetic field of up to 3 kOe and the spectral dependences of the TKE were measured in the range of 0.5–3.85 eV.

Mössbauer spectra from ^{57}Fe nuclei were taken using a MS-2020 spectrometer operating in a constant acceleration mode with a triangular shape of the time dependence of the source velocity relative to the absorber, namely, the film under study. As a source of γ quanta, ^{57}Co nuclei in Rh matrix with a radioactivity of 9 mCu were used. Mössbauer spectra were calibrated at room temperature with a standard α-Fe absorber. The processing and analysis of spectra were performed using methods for the model interpretation and determining the hyperfine parameter distributions by SpectrRelax software [18]. All measurements were carried out at room temperature.

3. Results and discussion

3.1. X-ray diffraction analysis

X-ray diffraction (XRD) patterns taken for the films under study are shown in Fig. 1; Table 1 gives the determined structure parameters. Full-

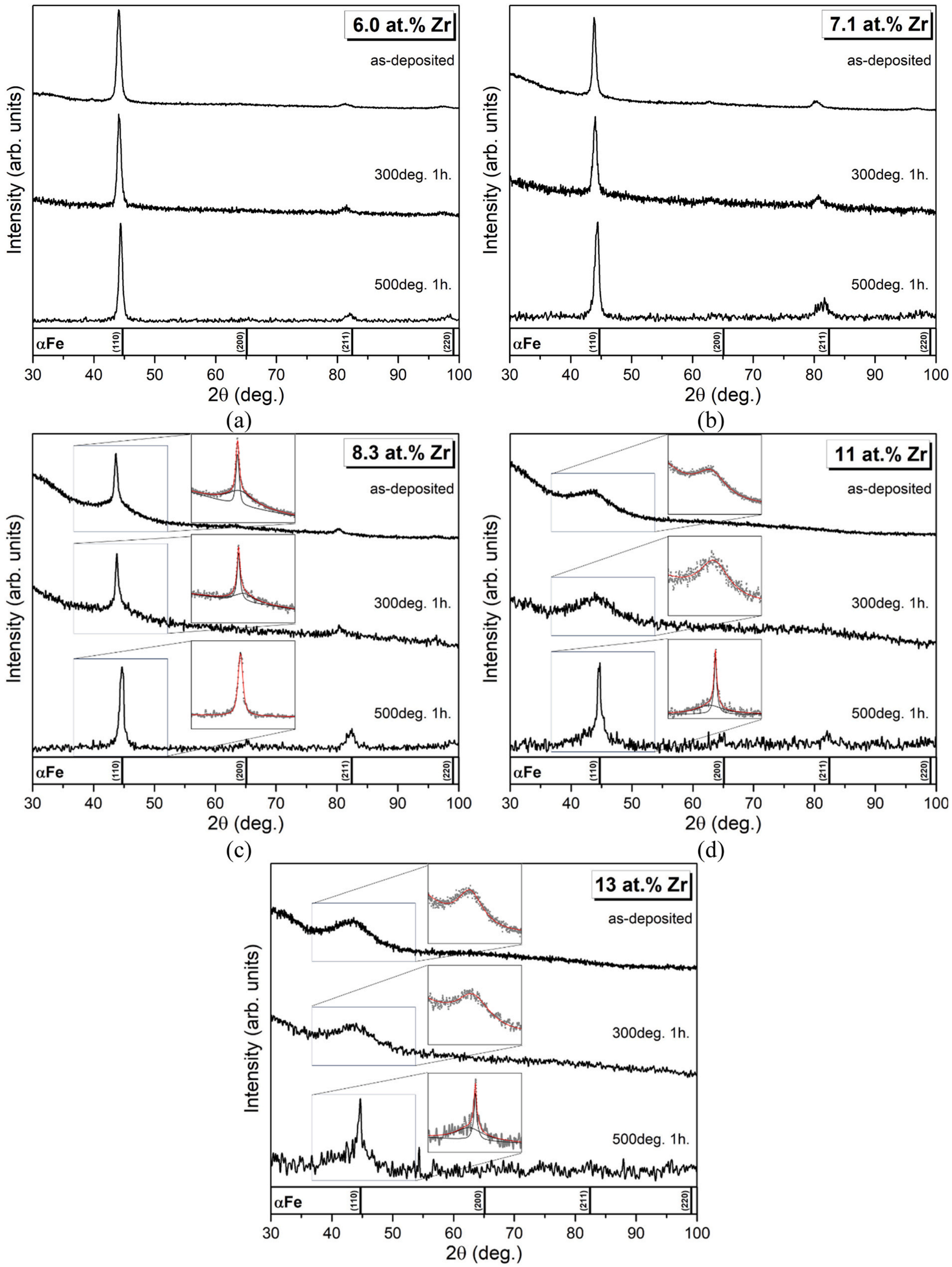

Fig. 1. XRD patterns of the as-deposited films with $x = 6.0$ (a), 7.1 (b), 8.3 (c), 11 (d), and 13 (e) and the films annealed at 300 and 500°C; the experimental X-ray reflection (grey symbol) near $2\theta \approx 44^\circ$ and its approximation (red curve) are shown. Insets demonstrate distinguishing the contributions of amorphous and crystalline constituents to the experimental X-ray reflection, which was performed using the Lorentzian function (wide black peaks, corresponding to the amorphous phase) and pseudo-Voigt function (narrow black peaks, corresponding to crystalline phase).

profile XRD patterns (Fig. 1a-c) taken for the films with $x = 6.0$, 7.1, and 8.3 demonstrate the intense reflection corresponding to $2\theta \approx 44^\circ$, weak reflection corresponding to $\approx 82^\circ$, and even a weaker reflection corresponding to $\approx 64^\circ$; the angular positions of the reflections are close to those of the (110), (200), and (211) reflections related to pure iron. This fact allows us to identify the crystalline state of the films characterized by a pronounced (110) axial texture along the normal to the film plane. The angular positions of the reflections are shifted to the 2θ low-angle range relative to the positions of the (110), (200) and (211) reflections of pure α-Fe; in this case, as the Zr content increases, the shift becomes more substantial. This fact suggests the formation of a phase with the body-centered cubic (bcc) structure with lattice parameters of 2.898, 2.926, and 2.929 Å for the films with $x = 6.0$, 7.1, and 8.3, respectively (Table 1), which exceed that of α-Fe (2.866 Å). The obtained data reveal the formation of the α-Fe(Zr) supersaturated solid solution, the degree of supersaturation of which increases with the Zr content in the film. Herein, the grain size D of this phase decreases from 20 nm (for the film with $x = 6.0$) to 7.2 nm (for the film with $x = 8.3$, Table 1) according to the mechanism of the solid solution strengthening.

In the case of the equilibrium Fe-Zr system [19], the Zr solubility in α-Fe is insignificant; it does not exceed 0.1 at%. Physical mechanisms underlying the formation of α-Fe(Zr) supersaturated solid solution under non-equilibrium conditions are considered in [20].

The nanocrystalline structure always contains an amorphous phase located within grain boundary areas. As the grain size decreases and grain boundaries become wider, the content of amorphous phase increases [6–8,21,22]. The formation of intergranular regions by the amorphous phase in nanocrystalline materials is the well-known fact established in numerous works [6–8,21,22]. This is confirmed by our transmission electron microscopy (TEM) studies on other Fe-based nanocrystalline films [5,23,24]. An amorphous structure of FeZr films of compositions close to $x \geq 11$ has been demonstrated by TEM in some publications [21,22].

We were not able to reveal the presence of the amorphous phase in the films with $x = 6.0$ and 7.1 by XRD. Mössbauer spectroscopy data (subSection 3.2) suggest the presence of the amorphous phase in the films.

X-ray diffraction patterns taken for the films with $x \geq 8.3$ demonstrate wide reflections localized in an angular range of $2\theta \approx 43$–45° (Fig. 1c-e), which are pronounced for the films with $x = 11$ and 13 (Fig. 1d, e). This fact allows us to conclude that the films with $x = 11$ and 13 are amorphous in terms of X-ray diffraction and to consider zirconium as an amorphizer for iron; the higher the Zr content, the higher the degree of amorphization of iron. The phase-structural state of the film with $x = 8.3$ is intermediate between the films with the lower and higher Zr content.

The experimental X-ray reflections near $2\theta \approx 43$–45° for the films with $x \geq 8.3$ (Fig. 1c-e, grey dots) were fitted (Fig. 1c-e, red line) and separated into (1) a wide peak corresponding to the amorphous phase using the Lorentzian function and (2) a narrow peak corresponding to crystalline phase using the pseudo-Voigt function (Fig. 1c-e, black curve). Note that the crystalline phase in these films is formed in the form of short-range ordered areas (CDs) or very fine grains which size, estimated by the Scherrer Eq. (1), is 2.4, 2.0, and 1.9 nm for the films with $x = 8.3$, 11, and 13, respectively (Table 1).

The obtained results agree well with fundamental knowledge on eutectic alloys. According to the equilibrium Fe-Zr phase diagram [19], the alloys with 8–10 at.% Zr correspond to the eutectic. The eutectic alloys have the constant low solidification temperature, and, therefore, prone to the supercooling during rapid cooling (quenching from the melt or vapor) and to the formation of amorphous structure. At a cooling rate of 10^{14} K (solidification from the vapor), in Fe-based films, the so-called amorphous structure in terms of X-ray diffraction forms, which is the Fe-rich amorphous matrix containing CDs or very fine grains enriched in Fe; the quantity of CDs/grains and their sizes depend on the preparation conditions and film composition [5,25–27].

The annealing of the films at 300 and 500°C leads to a modification of the XRD pattern observed for the as-deposited films (Fig. 1); the changes are clearer pronounced after annealing at 500°C. Positions of reflections of the bcc phase in the films with $x \leq 8.3$ become shifted toward high 2θ angles and approach positions for pure Fe; in this case, the intensity of (110) reflection increases. XRD patters of the films with $x = 11$ and 13 exhibit additional narrow reflections alongside with the wide reflection, which are observed at $2\theta \approx 44^\circ$ and $2\theta \approx 82^\circ$ and correspond to the (110) and (211) planes of the bcc lattice of the α-Fe-based phase. This demonstrates that the annealing of the films leads to a decrease in the amorphous phase content (crystallization process) and, therefore, to the increase in the crystalline phase content and decrease in the Zr content in the α-Fe(Zr) solid solution.

3.2. *Mössbauer spectroscopy*

In general, experimental Mössbauer spectra of the films are the combination of two subspectra, namely, magnetically ordered subspectrum (in the form of a sextet) and paramagnetic-type subspectrum (Fig. 2). According to the data given in Fig. 2, the as-deposited films with $x = 6.0$ and 7.1 comprise a considerable amount of magnetically ordered phase in contrast to the films with $x = 8.3$, 11, and 13, for which the Mössbauer spectra visually exhibit almost only paramagnetic-type subspectrum. After annealing at 500°C, the spectra of the films of the latter compositions exhibit the formation of magnetically ordered subspectra.

To choose the optimum fitting model for the Mössbauer spectra, using as an example the $Fe_{100-x}Zr_x$ film with $x = 7.1$, the hyperfine magnetic field distribution $p(H_n)$ at a ^{57}Fe

nucleus and quadrupole splitting distribution $p(\Delta)$ were reconstructed if there are possible linear correlations with the other hyperfine parameters of spectra. Fig. 3 shows the reconstruction result. The obtained hyperfine magnetic field distribution $p(H_n)$ and, therefore, the isomer shift distribution $p(\delta)$ for the spectrum (assuming the linear correlation between the isomer shift δ and hyperfine magnetic field H_n) allow us to conclude that the magnetically ordered subspectrum corresponds to the crystalline phase with the bcc structure (space group $Im\overline{3}m$), which, according XRD data (subsection 3.1), was identified as a metastable phase, namely, the supersaturated α-Fe(Zr) solid solution. The existence of almost equidistant local maxima in the $p(H_n)$ ($p(\delta)$) distribution, which can be assumed corresponding to different numbers of Zr atoms in the nearest environment of Fe atoms, attracts the attention. Note that the substitution of Fe atom for Zr atom in the nearest environment of Fe atoms leads to the decrease in both hyperfine field (in average by ≈ 30 kOe) and isomer shift of spectrum by ≈ 0.02 mm/s; in this case, the main peak (the most intense one) corresponds to a field of ≈ 330 kOe which almost coincides with that of pure α-Fe.

In the case of the film with $x = 7.1$, the paramagnetic-type subspectrum is described by a wide asymmetrical single-mode quadrupole splitting distribution $p(\Delta)$ with the average value $\Delta_{aver} = 0.448 \pm 0.028$ mm/s and the value $\Delta_{max} = 0.372 \pm 0.070$ mm/s corresponding to the distribution maximum (Fig. 3). The significant width of the distribution, namely ≈ 0.6 mm/s, is due to the local inhomogeneity of Fe atom environment in the regions being in the para- and superparamagnetic states.

When fitting all spectra of the $Fe_{100-x}Zr_x$ films, the method for reconstructing the distribution of quadrupole splitting $p(\Delta)$ was used for the reconstruction of the paramagnetic-type subspectrum, assuming the linear correlation of isomer shift δ with the quadrupole splitting Δ.

At the next stage of processing of Mössbauer spectrum for the film with $x = 7.1$, we used the model fitting for the magnetically ordered subspectrum (Fig. 4). The model is a combination of four Zeeman sextets differing in intensities I and hyperfine magnetic fields H_n. In this case, it was assumed that the δ isomer shifts and quadrupole shift ε of resonance lines for these sextets linearly depend on the number of Zr atoms in the

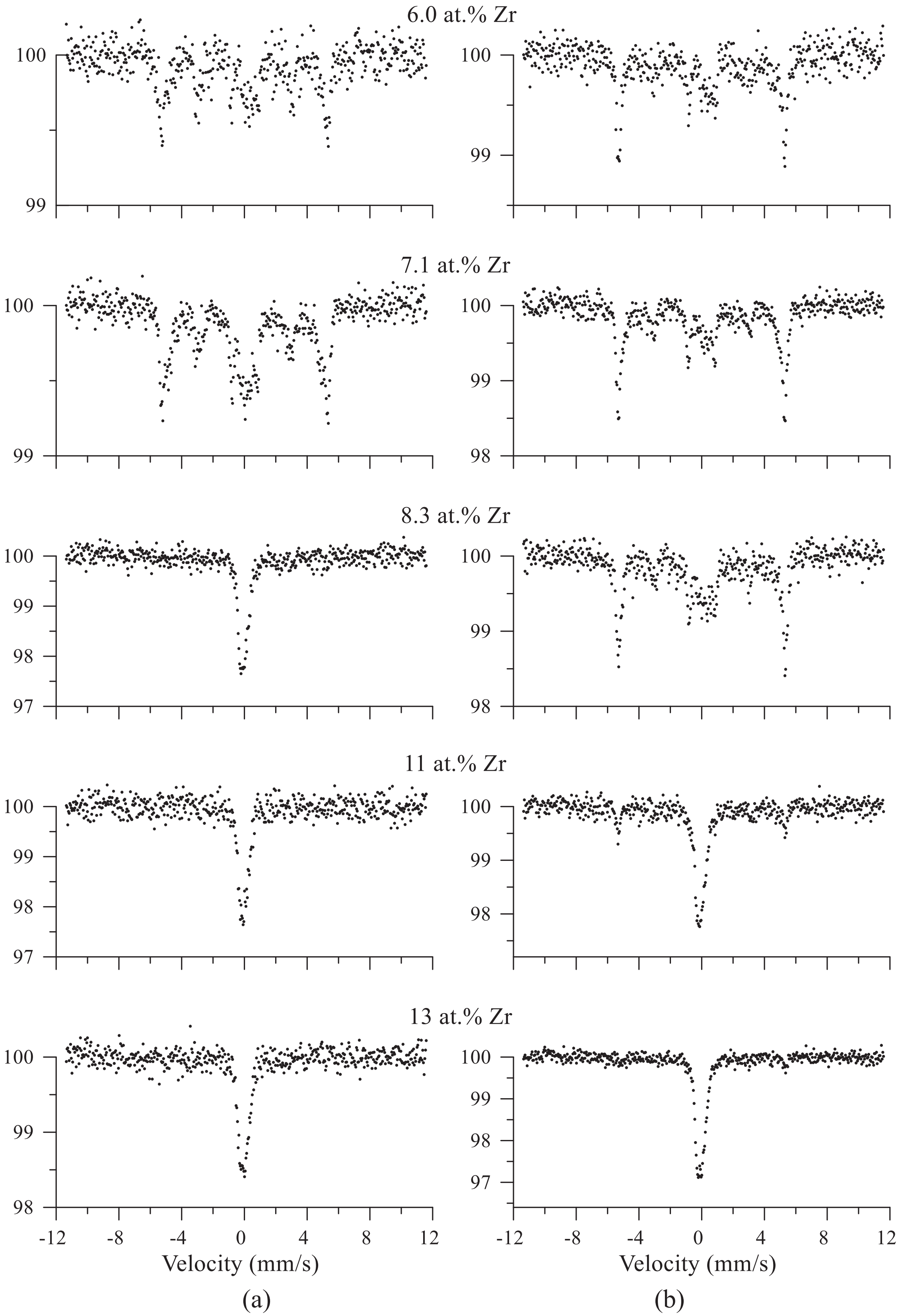

Fig. 2. Mössbauer transmission (%) spectra of the studied $Fe_{100-x}Zr_x$ films with different Zr content in the (a) as-deposited state and (b) after annealing at 500°C.

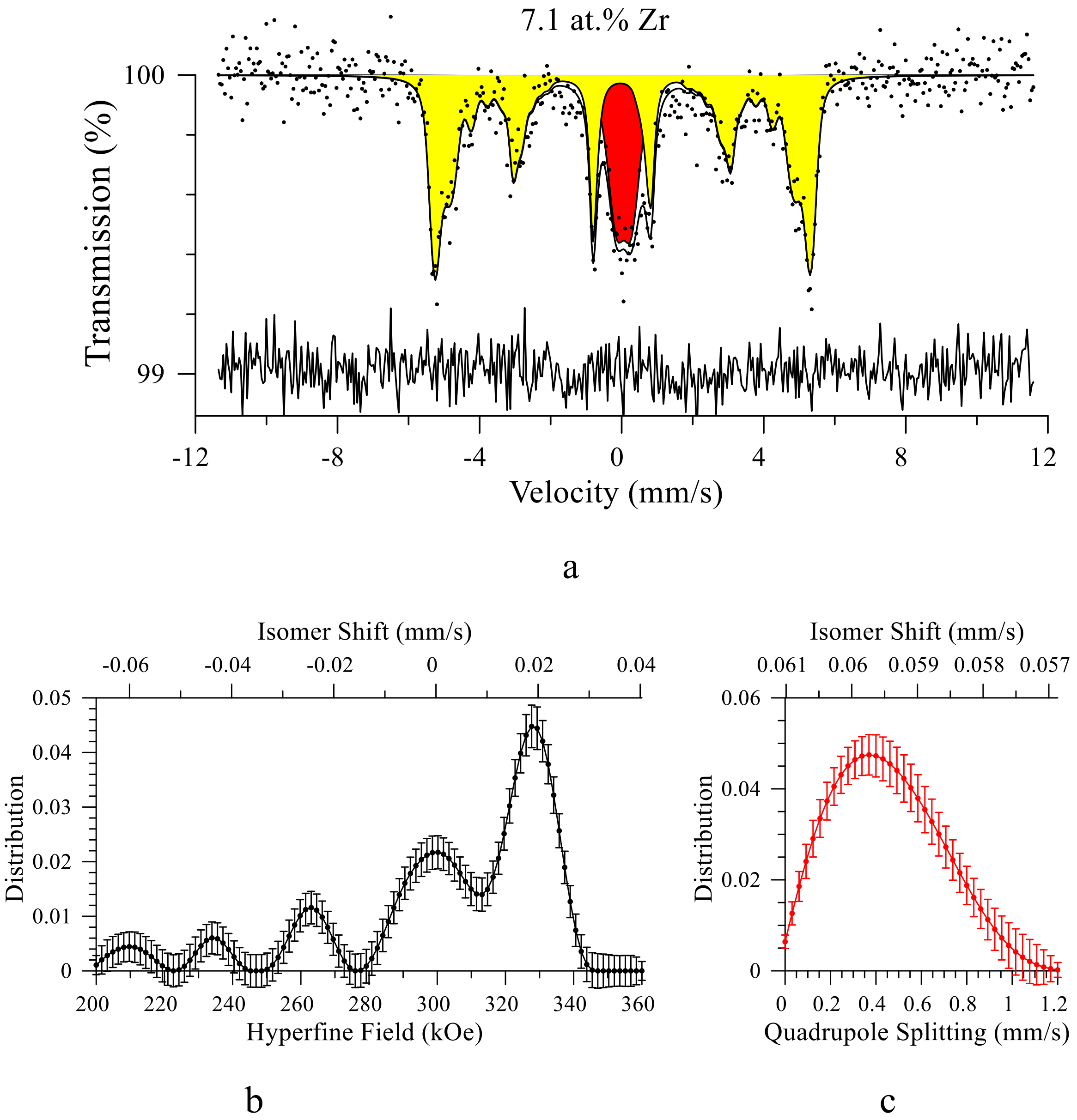

Fig. 3. (a) Mössbauer spectrum of the film with $x = 7.1$ and the result of its processing via reconstruction of distribution of hyperfine parameters of subspectra (the difference between the experimental and calculated spectra is shown under the experimental spectrum); reconstructed (b) hyperfine magnetic field $p(H_n)$ and (c) quadrupole splitting $p(\Delta)$ distributions.

nearest environment of Fe atoms.

It was found that the relative intensities of Zeeman sextets comprising the magnetically ordered subspectrum for the films with $x = 7.1$ correspond to the binomial distribution (Fig. 5), which means the almost random (equally probable) Zr atom distribution over Fe atom sites in the bcc lattice of α-Fe. Subsequently, the random (equally probable) Zr atom distribution over Fe atom sites was used in fitting all magnetically ordered subspectra. This allowed us to estimate the Zr atom concentration c_{Zr} in the α-Fe(Zr) crystalline phase formed in the films with $x \leq 7.1$ in the course of deposition and in the films with $x > 7.1$ after the annealing.

The model fitting of the magnetically ordered subspectrum for the film with $x = 7.1$ allowed us to obtain values of the hyperfine magnetic field $H_n(m)$ for each of Zeeman sextets. These values confirmed almost linear decrease in the field as the number m of Zr atoms in the nearest environment of Fe atom increases (Fig. 6): $H_n(m) = H_n(0) + \Delta H_n \cdot m$, with parameters $H_n(0) = 327.9 \pm 1.2$ kOe and $\Delta H_n = –30.3 \pm 1.7$ kOe.

In assuming the linear dependences of the spectral shift $\delta(m)$ and quadrupole shift $\varepsilon(m)$ of resonance lines of Zeeman sextets on the number m of Zr atoms in the nearest environment of Fe atom: $\delta(m) = \delta(0) + \Delta\delta \cdot m$, $\varepsilon(m) = \varepsilon(0) + \Delta\varepsilon \cdot m$, the following parameters were obtained: $\delta(0) = 0.017 \pm 0.006$ mm/s, $\Delta\delta = –0.023 \pm 0.012$ mm/s and $\varepsilon(0) = 0.012 \pm 0.006$ mm/s, and $\Delta\varepsilon = 0.008 \pm 0.012$ mm/s.

When processing the experimental spectra for the as-deposited (with $x = 8.3$, 11, and 13) and annealed (with $x = 11$ and 13) films, in which the relative contribution of magnetically ordered subspectrum was very low and almost not observed visually, it was assumed that, as the number m of Zr atoms in the nearest environment of Fe atom increases, the isomer shift decreases linearly from $\Delta\delta = –0.02$ mm/s, whereas the quadrupole shift remains unchanged ($\Delta\varepsilon = 0$ mm/s).

Fig. 7 shows the results of processing of the Mössbauer spectra for all films under study by model fitting of magnetically ordered subspectrum and the reconstruction of quadrupole splitting distribution for paramagnetic-type subspectrum. We can see that the description of spectra in terms of the used model fitting is quite successful.

To some extent, the magnetically ordered subspectrum

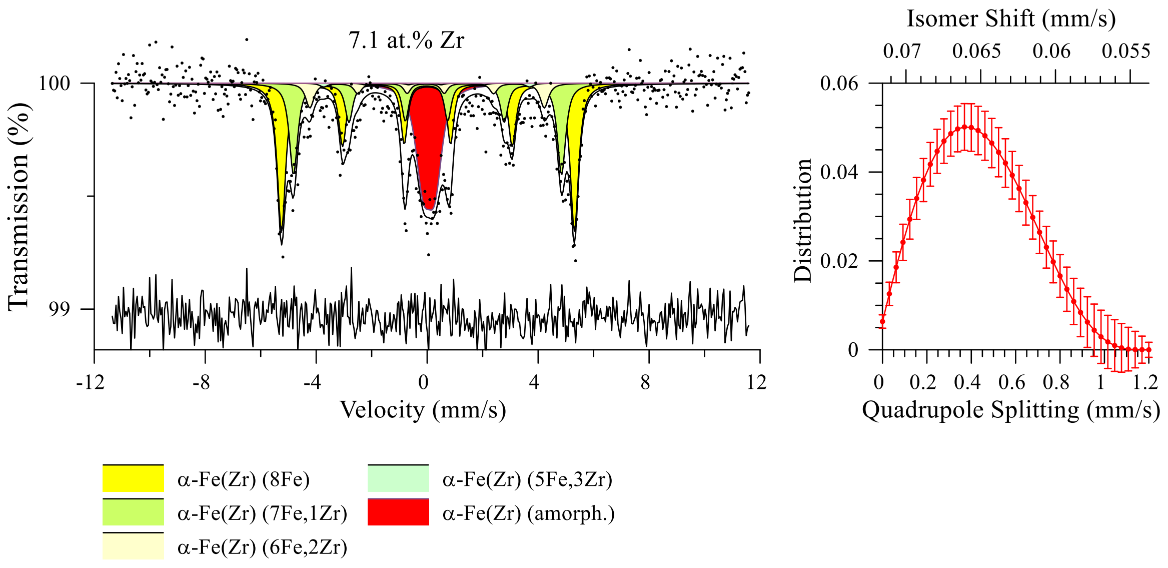

(a) (b)

Fig. 4. (a) Mössbauer spectrum of the film with $x = 7.1$ and the result of its processing with model fitting of magnetically ordered subspectrum and (b) reconstruction of quadrupole splitting distribution $p(\Delta)$ for paramagnetic-type subspectrum.

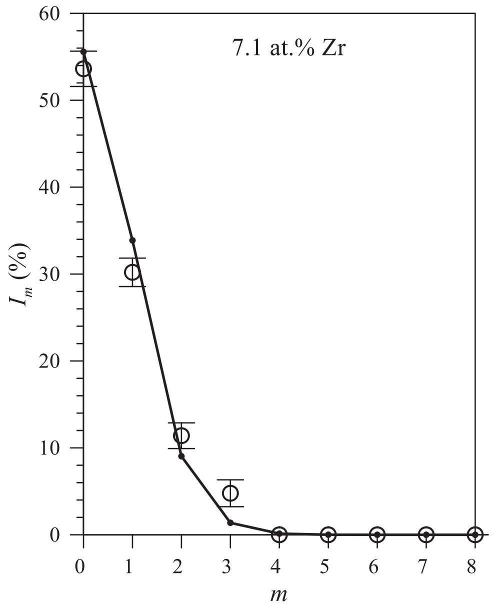

Fig. 5. Relative intensities $I(m)$ of Zeeman sextets comprising the magnetically ordered subspectrum vs. number of Zr atoms in the nearest environment of Fe atoms in the α-Fe(Zr) phase for the film with $x = 7.1$ (open circles) and binomial distribution for the same Zr concentration in the film (dots and solid lines).

corresponding to α-Fe(Zr)-phase crystallites is observed in the spectra of all as-deposited films; the relative intensity of the subspectrum (I_{magn}) decreases as the Zr concentration in the film increases (Fig. 8a). The abrupt decrease in the intensity I_{magn} is observed in passing from the film with $x = 7.1$ ($I_{magn} = 75.4 \pm 1.2$ %) to the film with $x = 8.3$ ($I_{magn} = 17.0 \pm 1.6$ %). The further increase in the Zr concentration leads to the decrease in the relative intensity I_{magn} down to 0 – 2 %. This is in a good agreement with the XRD data (subsection 3.1), which exhibit a decrease in the volume fraction of the crystalline phase and an increase in the volume fraction of the amorphous phase with increasing Zr content. The relative content of the α-Fe(Zr) phase largely determines the magnetic properties of the films (subsection 3.3).

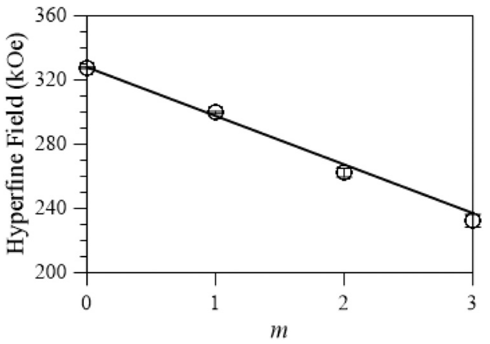

Fig. 6. Dependence of hyperfine magnetic field H_n on the number m of Zr atoms in the nearest environment of Fe atom in the α-Fe(Zr) phase for the film with $x = 7.1$.

The relative intensity I_{magn} for all films increases after annealing at 500°C and decreases as the Zr concentration increases (Fig. 8a). The intensity for the films with $x = 6.0$ and 7.1 increases only by 3 – 10 %, whereas for the films with $x = 8.3$, it abruptly increases from 17.0 ± 1.6 % to 76.2 ± 1.0 %. For the films with $x = 11$ and 13, which, in the as-deposited state, are characterized by very low content of the magnetically ordered α-Fe(Zr) phase, the increase in the intensity I_{magn} is ≈ 29 % and ≈ 10 %, respectively.

The Zr concentration c_{Zr} in the magnetically ordered α-Fe(Zr) phase in the as-deposited films with $x = 6.0$ and 7.1, which was determined by Mössbauer spectroscopy, turned out to be close to the Zr content in the film (black dots in Fig. 8b). For all films annealed at 500°C, an increase in the content of the magnetically ordered α-Fe(Zr) phase with the substantially lower Zr concentration c_{Zr}, as compared to the nominal Zr concentration in the film (Fig. 8b), is observed. The data on the decrease in the Zr concentration in the α-Fe(Zr) phase and increase in the content of the phase agree well with XRD data (subsection 3.1), according to which the annealing leads to the depletion of the supersaturated α-Fe (Zr) solid solution with Zr. The data obtained by both methods suggest that the annealing leads to the partial transformation of the metastable structure formed in the course of deposition toward the equilibrium state.

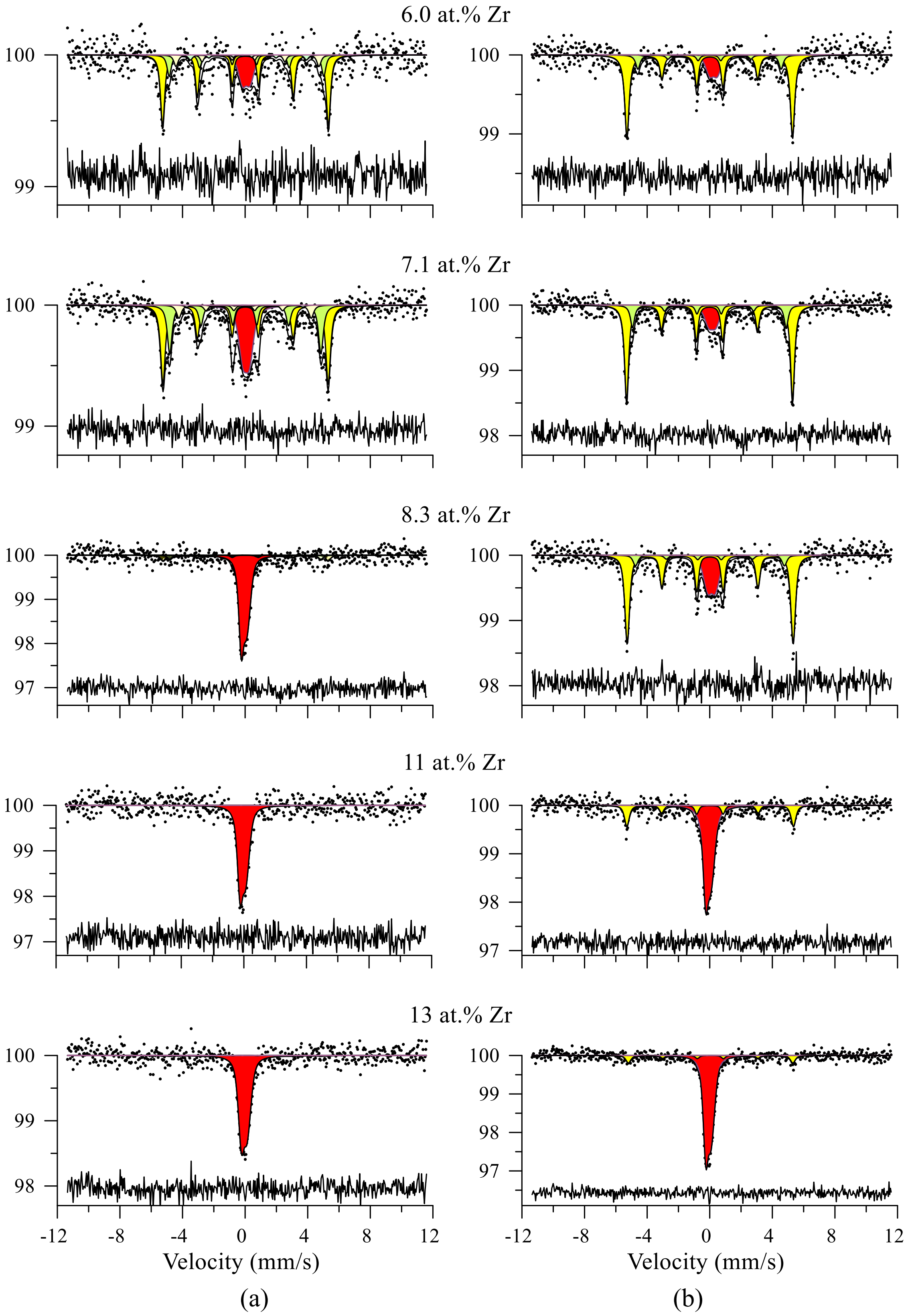

Fig. 7. Results of the processing of Mössbauer transmission (%) spectra of all studied (a) as-deposited films and (b) films annealed at 500 °C with the model fitting of magnetically ordered subspectrum and the reconstruction of quadrupole splitting distribution for paramagnetic-type subspectrum.

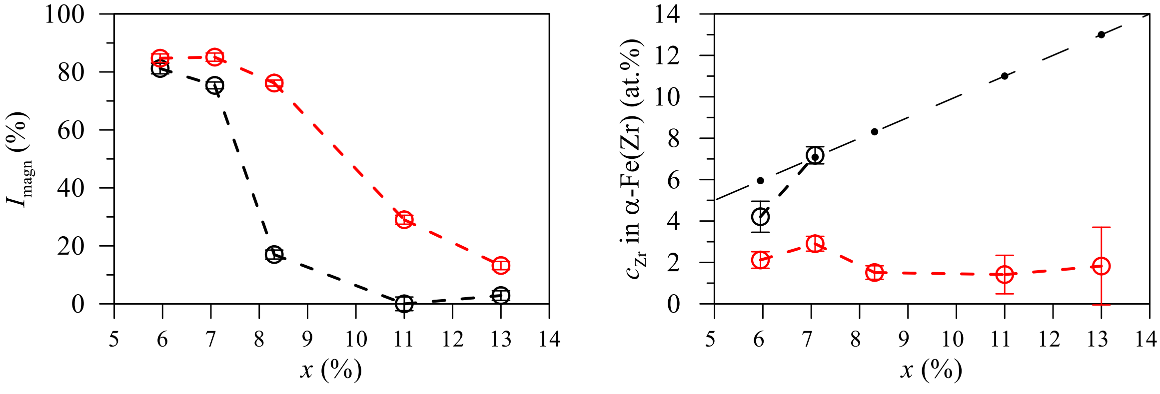

(a) (b)

Fig. 8. (a) Relative intensity I_{magn} of subspectrum of magnetically ordered α-Fe(Zr)-phase crystallites and (b) Zr concentration c_{Zr} in the α-Fe(Zr) phase in the $Fe_{100-x}Zr_x$ films in (black circles) as-deposited films and (red circles) films annealed at 500ºC vs. Zr content *x*; black points correspond to $c_{Zr} = x$.

Fig. 9 shows the concentration dependences of the average isomer shift and linear correlation coefficient Δ(δ)/Δ(Δ) between the shift δ and quadrupole splitting Δ for paramagnet-type subspectra in the spectra of as-deposited and annealed at 500ºC films.

The data presented in Fig. 9 indicate that the average values of the isomer shift for the as-deposited films with $x = 6.0$ and 7.1 and annealed films with $x = 6.0$, 7.1, and 8.3 are positive, whereas the linear correlation coefficients are almost zero (the corresponding data in Fig. 9 are shown with blue dashed rectangles). The paramagnetic-type subspectra with such parameters can be related to iron-containing phases being in paramagnetic and superparamagnetic states. Based on the spectrum intensities, the corresponding regions occupy a small part of film volume; it is likely that they correspond to amorphous interlayers between magnetically ordered regions characterized by the high Fe concentration (subsection 3.1). At the same time, the average isomer shift for the as-deposited films with $x = 8.3$, 11, and 13 and annealed films with c $x = 11$ and 13 is negative and equal to –0.05 mm/s, whereas the linear correlation coefficients Δ(δ)/Δ(Δ) are positive and equal to $\sim +0.15$ (the corresponding data in Fig. 9 are shown with green dashed rectangles). Such values of the parameters allow us to definitely relate the corresponding subspectra to the amorphous phase (see for example, [11, 28]). The existence of the positive correlation $\Delta(\delta)/\Delta(\Delta) > 0$ for these subspectra reveals the local inhomogeneity of nearest environment of Fe atoms, i.e., demonstrates the existence of amorphous state of Fe atoms. In this case, a correlated increase or decrease in the isomer shift (Fig. 9a) and in the quadrupole splitting (Fig. 9b) takes place at passing between Fe atomic sites. The former occurs due to a change in the electron density, and the latter occurs due to a change in the gradient of electric field resulting from the spatially nonuniform charge distribution of both itinerant electrons and ions in the vicinity of ^{57}Fe.

3.3. *Magnetometry*

All studied films are ferromagnets characterized by well-defined

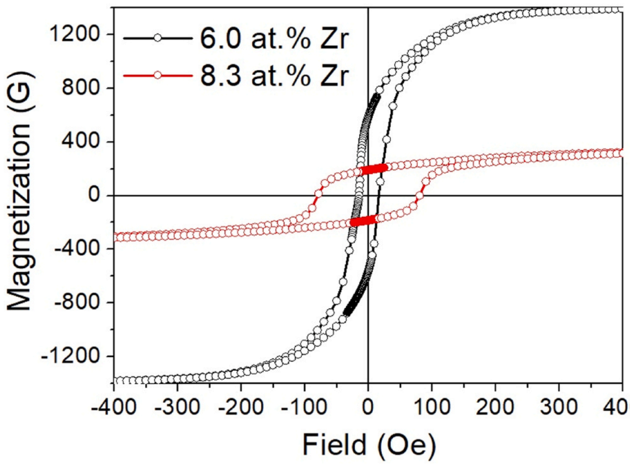

Fig. 10. Hysteresis loops of as-deposited $Fe_{100-x}Zr_x$ films with $x = 6.0$ and 8.3.

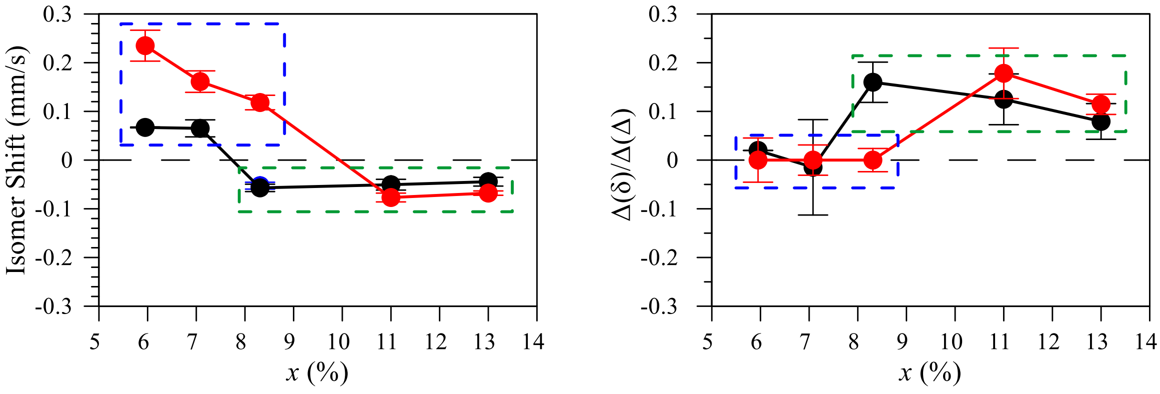

(a) (b)

Fig. 9. (a) Average isomer shift δ and (b) linear correlation coefficient Δ(δ)/Δ(Δ) between the isomer shift δ and quadrupole splitting Δ for paramagnetic-type subspectra in the spectra of (black circles) as-deposited and (red circles) annealed at 500ºC films vs. Zr concentration *x* (at%).

hysteresis loops measured by VSM (Fig. 10). The abrupt changes in the magnetic properties of the as-deposited films are observed for the films with $x = 7.1–8.3$, for which the saturation magnetization M_s undergoes a several-fold decrease, the coercive field H_c has the maximum, whereas the relative remanence M_r/M_s is less than 0.5 (Table 2). All the values imply the changes in the phase state of films with $x = 7.1–8.3$, which were demonstrated by XRD and Mössbauer spectroscopy data (subsections 3.1 and 3.2).

The films with $x = 6.0$ and 7.1 at% Zr are strong ferromagnets (Fig. 10) with the saturation magnetization M_s equal to 1420 and 1277 G, respectively; the hysteresis loops are closing at ~150 Oe, and the magnetization is saturated in relatively low fields (the approaching to saturation begins at less than 400 Oe). The films with $x = 8.3$, 11, and 13 are characterized by substantial fraction of paramagnetic phase, which manifests itself in the form of linear part of contribution to the magnetization curve (the effective susceptibility of entire sample, i.e., the film and substrate, is $\chi = (240-480)\bullet10^{-5}$). Note that, here and further on, it is impossible to distinguish the paramagnetic susceptibility of the film and that of diamagnetic substrate; because of this, all data on the measured magnetic parameters for the films are given after subtraction of paramagnetic contribution from the magnetization curve.

The saturation magnetization M_s of the films with $x = 8.3$, 11, and 13 decreases from 390 to 26 G. This is related to the formation of an increasing quantity of paramagnetic amorphous phase and decrease in the content of the ferromagnetic crystalline phase with increasing Zr concentration in the films. The values of the coercive field H_c (the maximum of which corresponds to $x = 8.3$) also reflect changes in the quantitative relationship between the crystalline and amorphous phases in these films.

Note that, for the films with $x = 8.3$, 11, and 13, the ferromagnetic hysteresis (Table 2) and the exchange interaction between CDs do not vanish (this is supported by the low coercive field H_c). This is evidence of the inhomogeneity of amorphous phase formed in the films, which is characterized by the presence of ferromagnetic regions in it. Such regions, as mentioned above, can have the form of relatively small aggregates of CDs or very fine grains (less than 1–2 nm in size), which are distributed over the amorphous Fe-based phase so that the possibility of exchange interaction between them is ensured, predetermining a low coercive field (Table 2) according to the random anisotropy model [8].

The annealing leads to a change in the magnetic properties of the films (Table 2) owing to the crystallization of the amorphous phase and depletion of the α-Fe(Zr) solid solution with respect to Zr (subsections 3.1 and 3.2). The saturation magnetization of the film with $x = 6.0$ changes slightly. The coercive field H_c increases about two times.

After annealing, a change in the shape of hysteresis loops of the films with $x = 7.1$ is qualitatively differs from that of the films with $x = 6.0$, namely, the uniaxial anisotropy field decreases, whereas the coercive field remains unchanged within the measurement error. The as-deposited films with $x = 8.3$ are characterized by the other crystalline-to-amorphous phase ratio as compared to that of the films with the lower Zr content; because of this, after annealing, they exhibit the other behavior, namely, the threefold increase in the saturation magnetization (Table 2) and the twofold decrease in the coercive field due to the increase in exchange interaction between grains of the crystalline phase.

Table 2
Static magnetic properties of the $Fe_{100-x}Zr_x$ films.

x, at%	T_{an}, °C	M_s, G	H_c, Oe	M_R/M_s
6.0	as-dep.	1420 ± 40	16 ± 7	0.39
	300	1498 ± 90	23 ± 7	0.42
	500	1400 ± 10	32 ± 5	0.29
7.1	as-dep.	1277 ± 60	41 ± 5	0.37
	300	1464 ± 20	37 ± 5	0.27
	500	1440 ± 25	36 ± 5	0.38
8.3	as-dep.	392 ± 10	80 ± 4	0.49
	300	671 ± 20	58 ± 5	0.37
	500	1260 ± 20	39 ± 5	0.22
11	as-dep.	39 ± 4	26 ± 5	0.41
	300	41 ± 2	24 ± 5	0.66
	500	513 ± 16	58 ± 5	0.23
13	as-dep.	26 ± 1	14 ± 5	0.42
	300	39 ± 4	26 ± 5	0.66
	500	229 ± 13	49 ± 5	0.33

The increase in the uniaxial anisotropy field after annealing, which is related to the crystallization arising in the amorphous phase, manifests itself also in the shape of hysteresis loops. Note that the low remanence M_r/M_s of the films can be related to, in particular, the existence of uniaxial anisotropy formed in the course of deposition.

The films with $x = 11$ and 13 exhibit the similar behavior. They demonstrate the abrupt changes in the magnetic properties after annealing (subsections 3.1 and 3.2). The saturation magnetization M_s of the as-deposited film with $x = 11$ is 39 G, which corresponds to a volume fraction of the α-Fe ferromagnetic phase of ~3 % (since the α-Fe(Zr) solid solution forms, and there is a possibility of presence of structural defects, the volume fraction of the ferromagnetic phase can be slightly higher). Ferromagnetic grains in these films are grouped to form stochastic domains [8]; this feature is supported by the low value of the coercive field $H_c = 26 \pm 5$ Oe.

Note that the annealing at 300°C does not lead to substantial changes in the saturation magnetization M_s and coercive field H_c of the ferromagnetic phase; this means that, at this temperature, the crystallization of the amorphous phase is rather faint, whereas after annealing at 500°C, the saturation magnetization M_s of the films with $x = 11$ and $x = 13$ increases by an order of magnitude and by several times, respectively; in this case, the values of these parameters remain moderate, namely, 513 ± 16 and 229 ± 13 G, respectively. The increase in the magnetization of the amorphous phase related to the exchange interaction between ferromagnetic CDs or between very fine grains, formed as a result of crystallization of the amorphous phase under corresponding time and temperature conditions of annealing, was considered in our previous study [5].

3.4. *Magneto-optical spectroscopy*

For metallic alloys, the magneto-optical (MO) response in the visible and near-infrared range is formed at a depth of 20–30 nm [29]; this fact allows one to study the magnetic properties of near-surface regions.

Fig. 11 shows MO spectra and field dependences of TKE of the films before and after annealing. Fig. 11a, in accordance with the structural studies (subsection 3.1, Table 1) and magnetic measurements (subsection 3.3, Table 2), shows abrupt changes in the magnetic properties of the as-deposited films with increasing x from 7.1 to 8.3. As is seen in Fig. 11a, the shape of MO spectra of the films with $x = 6.0$ and 7.1 is almost identical to that of nanocrystalline α-Fe, but differs only in the amplitude. This means that the magnetic constituent, which is responsible for MO signal, is the ferromagnetic nanocrystalline α-Fe(Zr) phase. However, already for the film with $x = 8.3$, i.e., as the Zr concentration increases only by 1.3 at%, the MO signal not only decreases by an order of magnitude but also changes its spectral profile; in this case, the wide peak typical of α-Fe and α-Fe(Zr) phases in a range near 2.0 eV disappears. Thus, the MO spectroscopy data definitely indicate a change in the magnetic and structural state of the films, namely, from typical ferromagnetic state of the nanocrystalline structure for the film with $x = 7.1$ to the paramagnetic state for the film with $x = 8.3$ with amorphous structure comprising ferromagnetic inclusions.

The magnetic field dependences of TKE for the films with $x = 6.0$ and 7.1 exhibit the saturation in low fields (Fig. 11c); this fact implies a slight amount of the paramagnetic phase or superparamagnetic particles, whereas the magnetization of the film with $x = 8.3$ increases linearly at high magnetic fields (inset in Fig. 11c). This fact means that in the structure of the film, alongside with easily magnetized nanocrystalline ferromagnetic Fe-based phase, a phase having the same or close composition exists, which is located within the paramagnetic

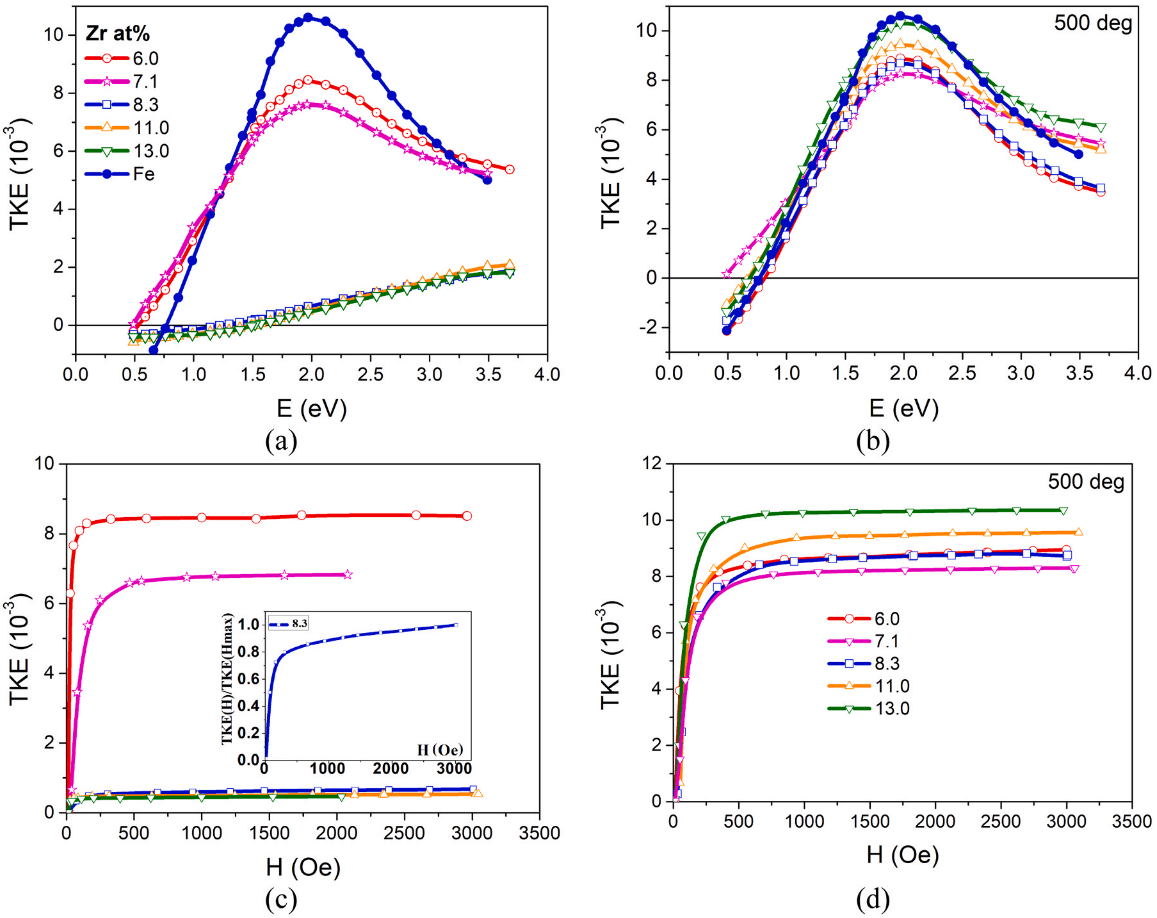

(a) (b) (c) (d)

Fig. 11. (a, b) Spectral and (c, d) field dependences of TKE for the $Fe_{100-x}Zr_x$ films differing in the Zr concentration in (a, c) as-deposited state and (b, d) after annealing at 500°C; inset in (c) shows the magnetic field dependence of $TKE(H)/TKE(H_{max})$ for the film with $x = 8.3$.

amorphous phase in the form of very fine grains and exhibits the superparamagnetic behavior. Therefore, the measured MO spectra and field dependences of TKE suggest the same transformation of the phase-structural state and magnetic properties near the surface and in the bulk (subsections 3.1–3.3). However, the differences also exist, which are considered below.

First, the comparison of field dependences of TKE in Fig. 11c and hysteresis loops measured with a vibrating-sample magnetometer (subsection 3.3 and Fig. 10) allows us to see that the saturation fields are different. In particular, the saturation field of TKE for the near-surface region of the film with $x = 6.0$ does not exceed 100–150 Oe (Fig. 11c), whereas for the entire film volume, it is 300–400 Oe (Fig. 10). This fact demonstrates the difference in the magnetic anisotropy fields for the near-surface region and the film bulk.

Second, according to the MO spectroscopy data, the maximum signal for the film with $x = 8.3$ at a field of 3.0 kOe at 2.0 eV is by about of eight times lower than that for the films with $x = 6.0$ and slightly differs from the maximum MO signal for the films with $x = 11.0$ (Fig. 11a). At the same time, the ratio of saturation magnetizations for the films with $x = 6.0$ and 8.3 is about 3 (see Table 2) and for the films with $x = 8.3$ and 11, is about 10. It is generally accepted that the MO signal is proportional to the magnetization [17]; therefore, such an unusual contradiction with the magnetic data calls for an explanation. The observed effect can be related to the fact that the content of the ferromagnetic phase in the near-surface layer in the film with $x = 8.3$ is lower than that far from the surface. In particular, this can be related to fact that a large amount of α-Fe-based phase fine grains is formed near the surface; these grains or their aggregates manifest themselves as superparamagnets. These regions are not saturated at a field of 3.0 kOe, in which the MO spectra were measured, and decrease the recorded MO signal (Fig. 11a). The existence of such superparamagnetic regions is seen just for the film with $x = 8.3$ rather than for the film with $x = 6.0$ both from the field dependences (inset of Fig. 11c) and Mössbauer spectroscopy data (Section 3.2). It is likely that the magnetic states of the near-surface region of the films with $x = 8.3$ and 11 are similar; this leads to insignificant differences in the MO signal for these compositions, whereas the resulting magnetizations differ by an order of magnitude. Note that the magnetically non-uniform state of the films, which is related to the formation of ferromagnetic regions differing in size and composition, leads to the fact that the MO signal can be not proportional to the magnetization. Recently, this fact was demonstrated in [17]. Indeed, the MO signal is determined by not only the magnetization but also the size, shape, and chemical composition of ferromagnetic regions (CDs, grains, or their aggregates) and their environment [17]. Because of this, the sum of MO signals of such ferromagnetic objects is not proportional to the total magnetization.

After annealing at 300°C, the MO spectra of the films with $x < 7.1$ are unchanged as compared to those for as-deposited state; however, the MO spectra for the films with $x > 7.1$ become similar to those for nanocrystalline films but exhibit a shift of the peak position (Fig. 12). As the Zr concentration in the film increases, the peak position shifts from 1.97 eV for α-Fe to 2.41 eV for the film with $x = 13$ (Fig. 12). Such a behavior of spectrum (Fig. 12) results from a superposition of the spectra for the film with $x < 7$ and the as-deposited film with $x > 8$ (see Fig. 11a), i.e., it follows from the shape of the MO spectrum for the films with $x > 8$ that, after annealing at 300°C, they comprise both the nanocrystalline ferromagnetic phase and small ferromagnetic regions located within the paramagnetic amorphous structural constituent. The

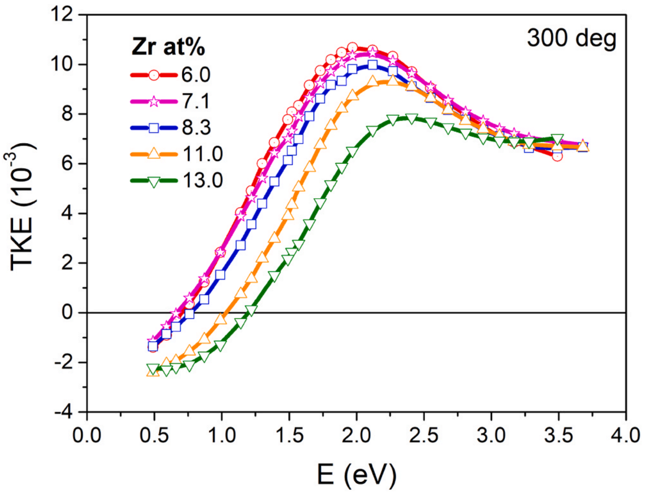

Fig. 12. Spectral dependences of the TKE for the $Fe_{100-x}Zr_x$ films differing in the Zr concentration annealed at 300°C.

annealing at 500°C leads to the further development of the crystallization of amorphous phase and disappearance of the shift of spectral peaks (Fig. 11b); the spectral profiles become similar to those of nanocrystalline α-Fe and α-Fe(Zr).

Note that, after annealing at 500°C, the maximum MO signal for the film with x = 13 becomes even higher than that for the nanocrystalline films with the low Zr content; for the films with $x = 11$ it is almost equal to that for nanocrystalline α-Fe (Fig. 11b). This suggests that Zr leaves the solid solution α-Fe(Zr); this is confirmed by XRD and Mössbauer spectroscopy data (subsections 3.1 and 3.2).

4. Conclusions

The comprehensive study of the phase and structural states, and magnetic properties of the $Fe_{100\text{-}x}Zr_x$ ($x = 6$–13 at%) films prepared by ion-beam deposition demonstrated that, at $x < 7$, the mixed (nanocrystalline + amorphous) structure forms, which consists of the dominant (in content) ferromagnetic nanocrystalline α-Fe(Zr) phase and paramagnetic amorphous areas; at $x > 8$, it transforms to the structure, which is presented by the main (in content) amorphous phase with ferromagnetic α-Fe(Zr)-phase regions (CDs, grains or their aggregates) ≤ 2 nm in size located within the amorphous phase. This change of the phase and structural states with increasing x from 7.1 to 8.3 leads to a several-fold decrease in the saturation magnetization and the MO response amplitude and to the change of the MO spectral profile as well. As x increases to 11 and further to 13, the relative amount of the amorphous phase increases. The annealing of the films leads to the decrease in content of paramagnetic constituent, increase in content of ferromagnetic constituent, and a change in its composition from α-Fe (Zr) to α-Fe. The combination of the data obtained by XRD, magnetometry, and by Mössbauer and magneto-optical spectroscopy allowed us to show that the ratio of amounts of the crystalline (ferromagnetic) and amorphous (paramagnetic) phases in the structure is determined by the Zr content in the films and its redistribution between phases in the course of annealing.

The difference of the magnetic properties in the near-surface region of films and in their bulk was discussed.

The obtained results suggest the possibility to purposefully control at the nanoscale the structural state of the Fe-Zr films with the nanocrystalline and/or amorphous structure in order to ensure the required level of magnetic properties.

Funding

The study was supported by the Russian Science Foundation (project no. 23–23–00434, https://rscf.ru/project/23–23–00434/) and performed using equipment acquired with the support of the Program for the development of the Lomonosov Moscow State University.

CRediT authorship contribution statement

E.N. Sheftel: Conceptualization, Supervision, Formal analysis, Visualization, Writing – original draft, Writing – review & editing. **V.S. Rusakov:** Investigation, Formal analysis, Writing – original draft. **E.A. Gan’shina:** Investigation, Formal analysis, Writing – original draft. **E.V. Harin:** Investigation, Formal analysis, Writing – original draft. **V.A. Tedzhetov:** Investigation, Formal analysis, Writing – original draft. **D. M. Gridin:** Investigation. **A.M. Gapochka:** Investigation. **I.M. Pripechenkov:** Investigation. **A.B. Granovsky:** Supervision, Writing – original draft, Writing – review & editing.

Declaration of Competing Interest

The authors declare that they have no known competing financial interests or personal relationships that could have appeared to influence the work reported in this paper.

Data Availability

Data will be made available on request.

References

[1] J. Zhou, J. You, K. Qiu, Advances in Fe-based amorphous/nanocrystalline alloys, J. Appl. Phys. 132 (4) (2022) 040702, https://doi.org/10.1063/5.0092662.

[2] E.N. Sheftel’, O.A. Bannykh, Nanocrystalline films of soft magnetic iron-based alloys, Russ. Metall. (Met.) 2006 (2006) 394–399, https://doi.org/10.1134/S0036029506050065.

[3] E.N. Sheftel, V.A. Tedzhetov, E.V. Harin, G.Sh Usmanova, Films with nanocomposite structure αFe(N) + ZrN for soft magnetic applications, Thin Solid Films 748 (2022) 139146, https://doi.org/10.1016/j.tsf.2022.139146.

[4] E.N. Sheftel, E.V. Harin, S.Yu Bobrovskii, K.N. Rozanov, V.A. Tedzhetov, I. O. Bannykh, Ph.V. Kiryukhantsev-Korneev, FeTiB nanocrystalline films: static and dynamic magnetic properties in accordance with phase composition and magnetic structure, J. Alloy. Compd. 968 (2023) 171981, https://doi.org/10.1016/j.jallcom.2023.171981.

[5] E.N. Sheftel, V.A. Tedzhetov, E.V. Harin, P.V. Kiryukhantsev-Korneev, O. M. Zhigalina, G.S. Usmanova, Magnetron-deposited FeTiB films: from structural metastability to the specific magnetic state, Coatings 14 (4) (2024) 475, https://doi.org/10.3390/coatings14040475.

[6] H. Gleiter, Nanostructured materials: state of the art and perspectives, Nanostr. Mater. 6 (1-4) (1995) 3–14, https://doi.org/10.1016/0965-9773(95)00025-9.

[7] R.A. Andrievski, A.M. Glezer, Size effects in properties of nanomaterials, Scr. Mater. 44 (8-9) (2001) 1621–1624, https://doi.org/10.1016/S1359-6462(01)00786-2.

[8] G. Herzer, Modern soft magnets: amorphous and nanocrystalline materials, Acta Mater. 61 (3) (2013) 718–734, https://doi.org/10.1016/j.actamat.2012.10.040.

[9] N. Saito, H. Hiroyoshi, K. Fukamichi, Y. Nakagawa, Mictomagnetism of Fe-rich Fe-Zr amorphous alloys studied by AC susceptibility in a superposed DC field, J. Phys. F: Met. Phys. 16 (1986) 911–919, https://doi.org/10.1088/0305-4608/16/7/018.

[10] J.J. Rhyne, R.W. Erwin, J.A. Fernandez-Baca, G.E. Fish, Magnetic correlations in amorphous Fe-Zr alloys, J. Appl. Phys. 63 (8) (1988) 4080–4082, https://doi.org/10.1063/1.340554.

[11] K.M. Unruh, C.L. Chien, Magnetic properties and hyperfine interactions in amorphous Fe-Zr alloys, Phys. Rev. B 30 (1984) 4968–4974, https://doi.org/10.1103/PhysRevB.30.4968.

[12] C. Michaelsen, E. Hellstern, Mössbauer effect on mechanically alloyed Fe-Zr glasses, J. Appl. Phys. 62 (1) (1987) 117–119, https://doi.org/10.1063/1.339168.

[13] H.M. Rietveld, A profile refinement method for nuclear and magnetic structures, J. Appl. Crystallogr. 2 (2) (1969) 65–71, https://doi.org/10.1107/S0021889869006558.

[14] A.L. Patterson, The Scherrer formula for X-Ray particle size determination, Phys. Rev. 56 (10) (1939) 978–982, https://doi.org/10.1103/PHYSREV.56.978.

[15] A.R. Stokes, A.J.C. Wilson, The diffraction of X-rays by distorted crystal aggregates – I, Proc. Phys. Soc. 56 (1944) 174–181, https://doi.org/10.1088/0959-5309%2F56%2F3%2F303.

[16] E.V. Shelekhov, T.A. Sviridova, Programs for X-ray analysis of polycrystals, Met. Sci. Heat. Treat. 42 (2000) 309–313, https://doi.org/10.1007/bf02471306.

[17] E.A. Gan'shina, V.V. Garshin, N.N. Perova, I.M. Pripechenkov, A.N. Yurasov, M. M. Yashin, V.V. Rylkov, A.B. Granovskii, Magneto-optical Kerr spectroscopy of nanocomposites, J. of Experim. Theoret. Phys 137 (2023) 572–581, https://doi.org/10.1134/S1063776123100151.

[18] M.E. Matsnev, V.S. Rusakov, SpectrRelax: An application for Mössbauer spectra modeling and fitting, AIP Conf. Proc. 1489 (1) (2012) 178–185, https://doi.org/10.1063/1.4759488.

[19] ASM Handbook, in: H. Okamoto, M.E. Schlesinger, E.M. Mueller (Eds.), Alloy Phase Diagrams, 3, ASM International, 2016, https://doi.org/10.31399/asm.hb.v03.9781627081634.

[20] E.N. Sheftel, V.A. Tedzhetov, E.V. Harin, G.Sh Usmanova, A.L. Dyachkov, FeZrN films: Role of dc magnetron sputtering conditions in the formation of their elemental and phase compositions, Thin Solid Films 698 (2020) 137876, https://doi.org/10.1016/j.tsf.2020.137876.

[21] P.T. Korelis, A. Liebig, M. Björck, B. Hjörvarsson, H. Lidbaum, K. Leifer, A. R. Wildes, Highly amorphous Fe90Zr10 thin films, and the influence of crystallites on the magnetism, Thin Solid Films 519 (2010) 404–409, https://doi.org/10.1016/j.tsf.2010.07.084.

[22] K.A. Darling, B.K. VanLeeuwen, C.C. Koch, R.O. Scattergood, Thermal stability of nanocrystalline Fe–Zr alloys, Mater. Sci. Eng. A 527 (2010) 3572–3580, https://doi.org/10.1016/j.msea.2010.02.043.

[23] O.M. Zhigalina, D.N. Khmelenin, E.N. Sheftel', G.Sh Usmanova, A.L. Vasil'ev, A. Carlsson, Electron microscopy of phase and structural transformations in soft magnetic nanocrystalline Fe–Zr–N films, Crystallogr. Rep. 58 (2013) 344–354, https://doi.org/10.1134/S1063774513020302.

[24] O.M. Zhigalina, D.N. Khmelenin, E.N. Sheftel, G.Sh Usmanova, M. Inoue, Evolution of the phase-structure state during annealing of Fe-ZrN films grown by magnetron sputtering, J. Surf. Investig. 4 (2010) 727–732, https://doi.org/10.1134/S1027451010050058.

[25] S.P. Gubin, Yu.A. Koksharov, G.B. Khomutov, G.Yu Yurkov, Magnetic nanoparticles: preparation, structure and properties, Russ. Chem. Rev. 74 (6) (2005) 489–520, https://doi.org/10.1070/RC2005v074n06ABEH000897.

[26] Guo-Ju Chen, Sheng-Rui Jian, Jason Shian-Ching Jang, Yung-Hui Shih, Yuan-Tsung Chen, Shien-Uang Jen, Jenh-Yih Juang, The effects of annealing temperature and sputtering power on the structure and magnetic properties of the Co-Fe-Zr-B thin films, Intermetallics 30 (2012) 127–131, https://doi.org/10.1016/j.intermet.2012.03.017.

[27] E.N. Sheftel, V.A. Tedzhetov, E.V. Harin, P.V. Kiryukhantsev-Korneev, G. S. Usmanova, O.M. Zhigalina, FeZrN Films: magnetic and mechanical properties relative to the phase-structural state, Materials 15 (1) (2022) 137, https://doi.org/10.3390/ma15010137.

[28] S.M. Fries, C.L. Chien, J. Crummenauer, H.-G. Wagner, U. Gonser, Mixed hyperfine interaction in amorphous Fe-Zr sputtered films in external magnetic field – A^{57}Fe Mössbauer study, Hyperfine Interact. 27 (1986) 405–408, https://doi.org/10.1007/BF02354792.

[29] G. Traeger, L. Wenzel, A. Hubert, Computer experiments on the information depth and the figure of merit in magnetooptics, Phys. Status Solidi (a) 131 (1) (1992) 201–227, https://doi.org/10.1002/pssa.2211310131.